Pusher-Propeller Blade Loading With and Without Pylon Trailing-Edge Blowing

Sinnige, Tomas; Ragni, Daniele; Eitelberg, Georg; Veldhuis, Leo

DOI
10.2514/6.2016-3421

Publication date
2016

Document Version
Accepted author manuscript

Published in
34th AIAA Applied Aerodynamics Conference

Pusher-Propeller Blade Loading With and Without Pylon Trailing-Edge Blowing

Tomas Sinnige*, Daniele Ragni†, Georg Eitelberg‡, and Leo L. M. Veldhuis§
Delft University of Technology, Delft, 2629 HS, the Netherlands

The aerodynamic interaction effects characteristic of pusher propellers were studied at the Large Low-Speed Facility of the German–Dutch wind tunnels (DNW-LLF). A propeller model was positioned downstream of a pylon equipped with a trailing-edge blowing system. Surface-pressure transducers integrated into the propeller blades confirmed the local impact of the pylon wake on the blade loads. At an intermediate thrust setting, the sectional lift impulsively increased by 30% during the wake passage. The application of pylon blowing decreased the integral velocity deficit in the pylon wake by up to 77% compared to the unblown case. As a result, the load fluctuations during the wake encounter were practically eliminated, thereby mitigating the adverse installation effects.

I. Introduction

ADVANCED propeller propulsion systems promise to offer an increase in propulsive efficiency compared to turbofans. Cabin-noise constraints and ground-clearance issues prompt propeller-aircraft designs with rear-mounted pusher propellers.[1] In such a configuration, the inflow to the propeller is perturbed by the pylon wake. The momentum deficit downstream of the pylon is experienced by the blades as a periodic local reduction in inflow velocity, as illustrated in Fig. 1. Consequently, the blade-section inflow angles vary during the wake passage, resulting in unsteady blade loads and associated increased propeller noise emissions.[2]

The presence of the unsteady blade loads was confirmed by flight tests with a pylon-mounted pusher propeller equipped with high-frequency pressure transducers, as reported by Farokhi et al.[3,4] The pylon-installation impact was observed as a negative pressure pulse occurring over a large part of the propeller blade's suction surface.[3] Frequency analysis of the measured time histories led to the conclusion that the pylon–propeller interaction featured periodic leading-edge vortex formation and associated vortex shedding from the trailing edge.[4]

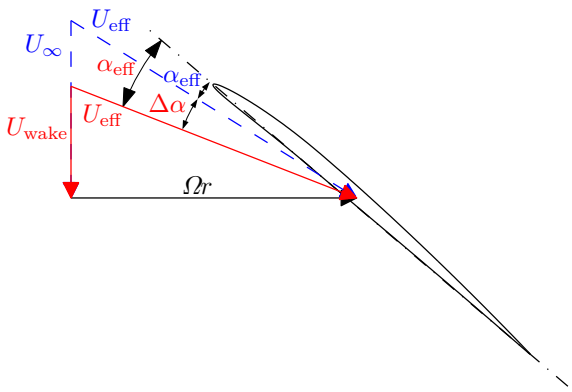

Figure 1. Schematic illustrating the angle-of-attack perturbation caused by the velocity deficit in the pylon wake.

The adverse pylon-installation effects can be mitigated by eliminating the momentum deficit in the pylon wake. This can be achieved using pylon blowing, as confirmed previously by experimental research with single-rotating[5–7] and contra-rotating[8–11] propellers, as well as numerical investigations[12]. The experimental studies published so far focused on the beneficial effects of pylon blowing on the far-field noise levels. The aerodynamic characteristics of the interaction, however, are still unclear. The experimental investigation discussed in the present paper aims at quantifying these aerodynamic installation effects by analysis of the propeller blade loads, with and without pylon trailing-edge blowing.

*Ph.D. Candidate, Flight Performance and Propulsion Section, Faculty of Aerospace Engineering, AIAA member.
†Assistant Professor, Wind Energy Section, Faculty of Aerospace Engineering, AIAA member.
‡Full Professor, Flight Performance and Propulsion Section, Faculty of Aerospace Engineering, AIAA member.
§Full Professor, Head of Flight Performance and Propulsion Section, Faculty of Aerospace Engineering, AIAA Member.

II. Experimental Setup

The test campaign was performed at the Large Low-Speed Facility of the German–Dutch wind tunnels (DNW-LLF). In the selected open-jet configuration with 8 m x 6 m outlet, the tunnel allows a wind-speed range of $0-80$ m/s. The turbulence levels in the longitudinal and lateral directions equal 0.24% and 0.13%, respectively. A semi-installed pusher-propeller configuration was simulated by positioning a powered tractor-propeller model downstream of a pylon equipped with a trailing-edge blowing system. Tests were performed with and without the pylon installed. A photograph of the test setup is shown in Fig. 2.

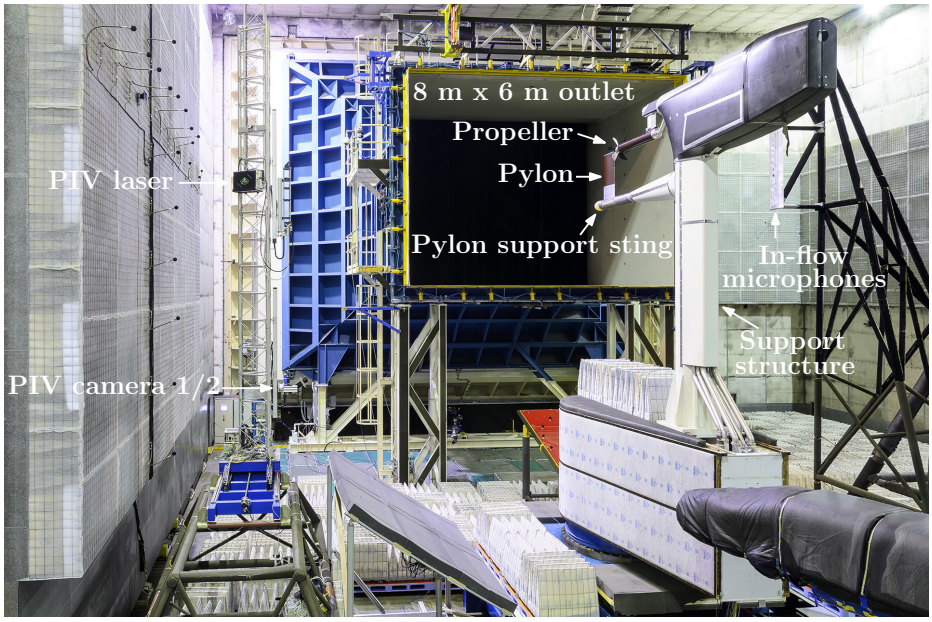

Figure 2. Overview of the experimental setup.

The six-bladed propeller model (Fig. 3) featured a rotor diameter of 0.508 m, and was designed and built for the European APIAN (Advanced Propulsion Integration Aerodynamics and Noise) research project[13–16]. The blade angle at 75% of the radius was set to 40.4 degrees. A six-component rotating shaft balance (RSB) was integrated into the propeller model, while four of the blades were equipped with a total of 27 miniature surface-pressure transducers. This paper describes the results acquired at a radial station of $r/R \approx 0.65$. The fourteen sensors available at this radial position were equally distributed over the pressure and suction sides of the blade, covering a chordwise range of 5% to 90% of the local chord (Fig. 4). The surface-pressure sensors had a frequency response of $0-10$ kHz. The recorded data were processed using a phase-averaging technique based on a one-pulse-per-revolution trigger signal. The circumferential blade position ϕ was defined as indicated in Fig. 5.

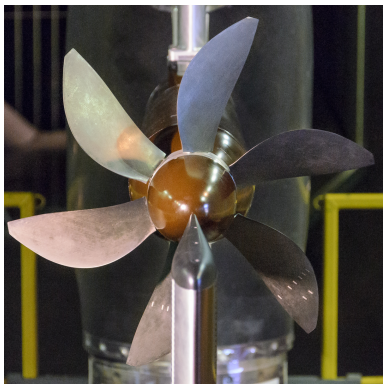

Figure 3. APIAN propeller model installed downstream of the pylon model.

Figure 4. Surface-pressure transducers integrated into the propeller blade at $r/R \approx 0.65$.

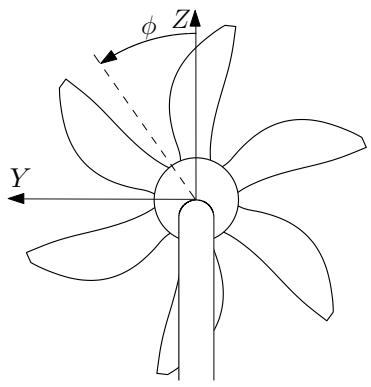

Figure 5. Reference system used to define the circumferential blade position.

The pylon model (Fig. 6) was manufactured by extrusion of a NACA 0010 profile into a straight wing of 0.489 m chord and 0.900 m span. The trailing-edge thickness was increased to 0.8% of the chord to allow for the installation of the blowing system. The pylon was positioned at a fixed spacing of approximately 30% of the propeller diameter upstream of the propeller. A pylon-blowing system was installed in the aft part of the pylon, with its outlet integrated into the trailing edge. The design of the system and the uniformity of its outflow were discussed previously in Ref. 7. Measurements were taken at different blowing rates to assess the sensitivity of the pylon-installation effects to the degree of wake filling. A pylon-blowing mass-flow coefficient $c_{\dot{m}}$ was introduced as the ratio between the blown and free-stream mass flows (referenced to the outflow area of the blowing slit).

Figure 6. Pylon model installed upstream of the propeller model.

Stereoscopic particle-image velocimetry (sPIV) was employed to measure the velocity deficit in the flow field behind the pylon trailing edge. An overview of the most important parameters of the sPIV setup and data-acquisition characteristics was provided in Ref. 7. Figure 7 depicts a schematic of the measurement-plane locations relative to the pylon and the propeller.

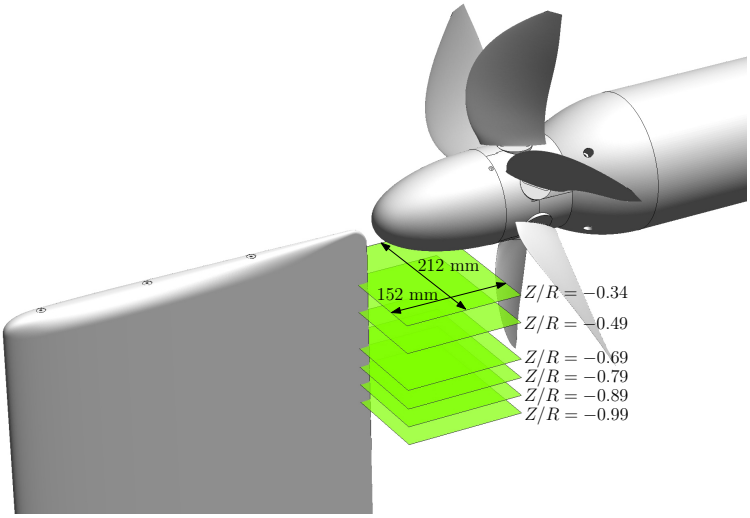

Figure 7. Schematic indicating the locations of the sPIV measurement planes.

All results discussed in the present paper were obtained at a free-stream velocity of $U_\infty = 60$ m/s. The propeller was operated at low, intermediate, and high thrust settings, corresponding to advance ratios of 1.75, 1.40, and 1.05, respectively. The associated thrust coefficients ($C_T = T\rho_\infty^{-1}n^{-2}D^{-4}$) equaled 0.18, 0.36, and 0.51. Symmetric inflow conditions ($\alpha = \beta = 0°$) were considered only. Before the start of the final test program, the propeller noise emissions were evaluated at a single operating point for a full range of blowing rates. The blowing coefficient resulting in the largest noise reductions was selected for the subsequent measurements with blowing enabled ($c_{\dot{m}} = 1.6$), together with blowing coefficients equal to 85% and 115% of the optimum ($c_{\dot{m}} = 1.4$ and $c_{\dot{m}} = 1.8$). Moreover, a zero-blowing case ($c_{\dot{m}} = 0.0$) was considered as baseline configuration to which the results with blowing enabled could be compared.

III. Results

The pusher-propeller installation effects are caused by the perturbation of the propeller inflow by the pylon wake. Therefore, the measurements of the flow fields between the pylon and the propeller are treated first. Subsequently, the resulting unsteady propeller response is considered, both in terms of the sectional and integral blade loads.

A. Propeller Inflow

The sPIV setup was used to obtain quantitative information of the propeller inflow. Figure 8 presents the averaged pylon-wake velocity fields for the unblown and blown configurations, acquired at an intermediate thrust setting ($J = 1.40$). The results measured with blowing enabled were obtained at the optimal blowing rate corresponding to $c_{\dot{m}} = 1.6$.

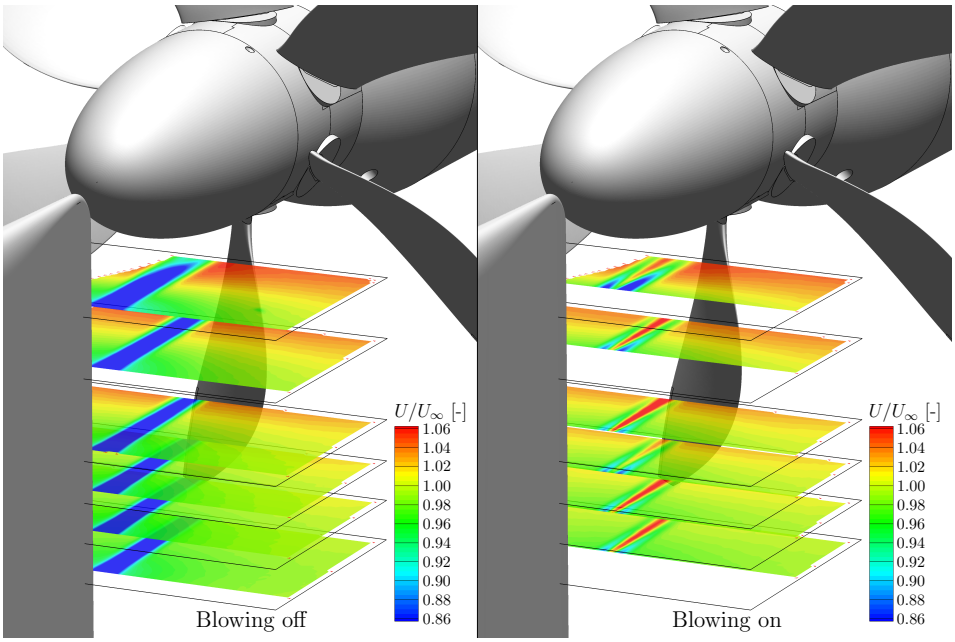

Figure 8. Pylon-wake velocity fields for the unblown and blown ($c_{\dot{m}} = 1.6$) configurations; $J = 1.40$.

Figure 8 shows that the velocity deficit in the pylon wake was considerably decreased by the application of blowing. Furthermore, the suction by the propeller can be recognized as a velocity increase towards the propeller. To gain more insight into the propeller inflow, Fig. 9 depicts the velocity profiles extracted at the most downstream position in the field of view, located at 0.07 times the propeller diameter upstream of the propeller ($\Delta X/D = 0.07$). Linear interpolation was performed between the measurement planes to extract the axial velocity experienced by a blade section at $r/R \approx 0.65$, for the pylon-off and pylon-installed configurations. An integral velocity deficit parameter ξ was defined to quantify the deficit in the wake region:

$$\xi = \frac{1}{\phi_\mathrm{R} - \phi_\mathrm{L}} \int_{\phi_\mathrm{L}}^{\phi_\mathrm{R}} \left| 1 - \frac{U_\mathrm{Pylon\text{-}on}}{U_\mathrm{Pylon\text{-}off}} \right| \mathrm{d}\phi, \tag{1}$$

with ϕ_L and ϕ_R the circumferential integration limits, selected as $\phi_\mathrm{L} = 174°$ and $\phi_\mathrm{R} = 186°$.

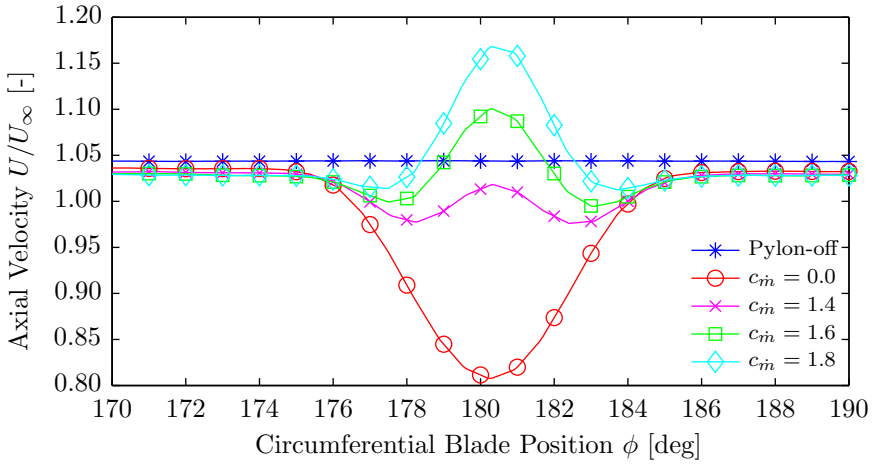

Figure 9. Propeller-inflow velocity profiles at $\Delta X/D = 0.07$; $r/R \approx 0.65$, $J = 1.40$.

Figure 9 confirms the reduction of the velocity deficit in the pylon wake achieved by blowing. At the optimal blowing coefficient ($c_{\dot{m}} = 1.6$), the integral velocity deficit was 77% lower than for the unblown configuration. The velocity overshoot on the wake centerline was the result of suboptimal mixing between the external flow and the blown jet. This was due to the thin blowing slit in the pylon trailing edge and the limited distance between the pylon and the propeller. Compared to the pylon-off configuration, the cases with the pylon installed showed a slightly reduced velocity outside of the wake region. This was due to the inviscid effect of the pylon on the surrounding flow field. The offset was slightly asymmetric with respect to the wake centerline due to a small angularity of the inflow, attributed to interference with the in-flow measurement infrastructure or a slight misalignment of the test setup.

B. Sectional Blade Loads

The locally reduced inflow velocity in the pylon-wake region leads to a sudden angle-of-attack increase experienced by the blade sections. The surface-pressure transducers integrated into the propeller blades were used to quantify the resulting impact on the sectional blade loads.

As a first step, the pressure distributions on the blades of the isolated propeller are considered. Figure 10 presents the results acquired at a radial coordinate of $r/R \approx 0.65$, as a function of the propeller thrust setting. The time-averaged signals are shown, as measured during 17 to 24 repeated runs per thrust condition. The pressure coefficient was defined relative to the effective dynamic pressure in the rotating frame. The standard deviation of the mean pressure-coefficient measurements was less than 0.01, at all operating conditions considered. The pressure difference across the blade was integrated in the chordwise direction to obtain the sectional lift coefficient. The resulting data are provided in Table 1.

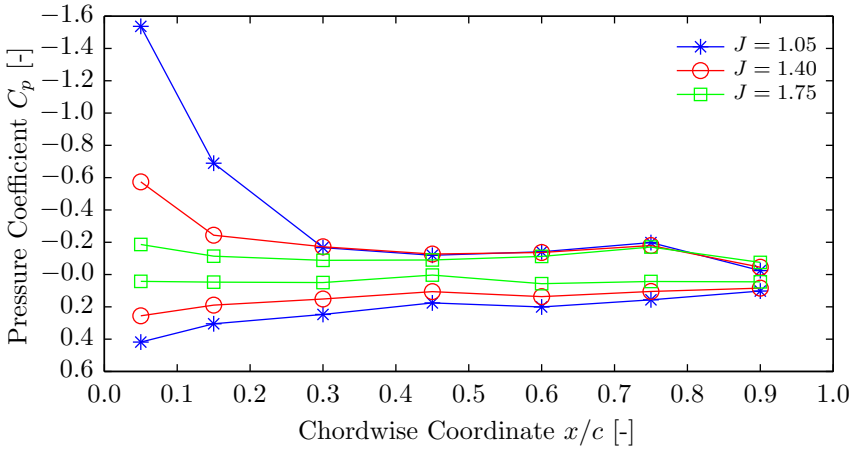

Figure 10. Blade pressure distributions for the isolated propeller; $r/R \approx 0.65$.

Table 1. Sectional lift coefficients for the isolated propeller; $r/R \approx 0.65$.

J	c_l
1.05	0.497 ± 0.001
1.40	0.300 ± 0.001
1.75	0.144 ± 0.002

Figure 10 and Table 1 confirm the expected increase in blade loading with decreasing advance ratio, hence increasing thrust setting. The angles of attack of the sections increase when the advance ratio is decreased, resulting in a stronger suction peak. The pressure distribution on the aft part of the blade's suction side hardly changed with advance ratio.

To assess the modification of the sectional loading caused by the installation of the pylon, Fig. 11 depicts the phase-averaged pressure distributions for the pylon-off and pylon-installed configurations, with and without blowing. Data are presented for three circumferential blade positions, defined relative to the leading edge of the blade at $r/R \approx 0.65$. The three angles correspond to the location of peak impingement impact, together with circumferential positions twenty degrees before and after. The unsteady nature of the interaction problem caused a phase lag between the position of the maximum blade-loading change ($\phi = 183°$) and that of the maximum velocity deficit in the wake ($\phi \approx 180°$).

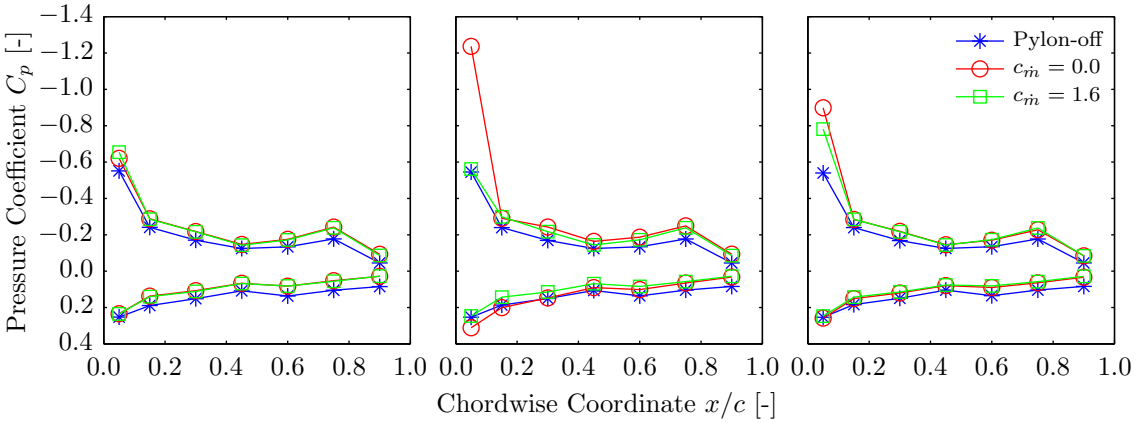

Figure 11. Effect of pylon installation on the unsteady blade pressure distributions; $r/R \approx 0.65$, $J = 1.40$.

The results plotted in Fig. 11 highlight the change of the pressure distribution due to the installation of the unblown pylon. At the circumferential blade position of the maximum wake impact ($\phi = 183°$), the suction-peak pressure coefficient was double that of the value observed for the pylon-off configuration. Application of the blowing system significantly reduced the severity of the interaction effects, resulting in a pressure distribution comparable to that of the isolated propeller. After the wake impingement ($\phi = 203°$), the differences between the pressure distributions for the cases with and without the pylon installed were due to the modification of the flow field outside of the wake region, as discussed under Fig. 9.

The interaction effects caused by the pylon-wake encounter were most pronounced at the chordwise position closest to the leading edge of the blade ($x/c = 0.05$). Figures 12 and 13 present time histories of the phase-averaged pressure coefficient measured at this position on the suction and pressure sides of the blade.

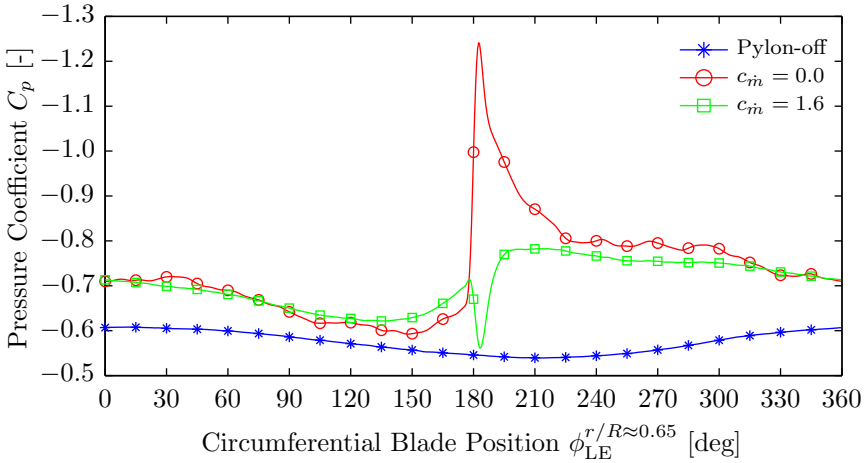

Figure 12. Effect of pylon installation on the suction-side pressure peak; $x/c = 0.05$, $r/R \approx 0.65$, $J = 1.40$.

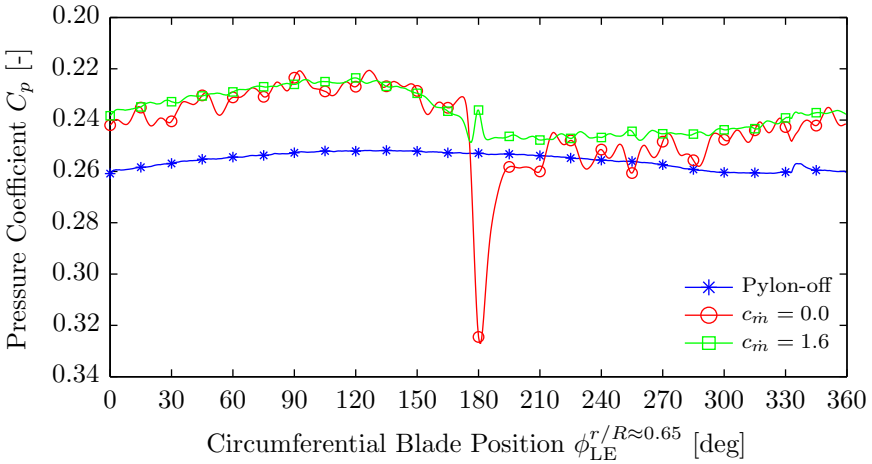

Figure 13. Effect of pylon installation on the pressure-side pressure peak; $x/c = 0.05$, $r/R \approx 0.65$, $J = 1.40$.

Figures 12 and 13 show the impulsive effect of the pylon-wake encounter on the pressure near the leading edge of the blade. Without blowing, the magnitude of the pressure coefficient increased on the suction and pressure sides of the blade due to the sudden angle-of-attack increase during the wake passage. The pressure perturbation first occurred at a circumferential angle of about $\phi = 174°$, matching with the position of the edge of the pylon wake (Fig. 9). As discussed before, the peak pressure disturbance occurred after the position of maximum velocity deficit because of the unsteady nature of the perturbation problem. After the peak impact, a more gradual recovery occurred towards the levels outside of the pylon wake region. As a result, the circumferential extent of the pressure disturbance was larger than that of the pylon wake.

Application of the blowing system decreased the pressure fluctuations in the wake region. The remaining non-uniformities were due to the velocity overshoot on the blown pylon's wake centerline (Fig. 9). The data for the pylon-off configuration displayed a small angle-of-incidence effect, most likely due to the slight flow angularity discussed before. The offset in mean levels between the pylon-off and pylon-installed configurations was attributed to a shift of the sensor calibration factor, which could not be corrected for.

The modification of the pressure distribution due to the pylon-installation effects directly translates into fluctuating blade loads. Figure 14 presents the sectional lift coefficient as a function of the circumferential blade position, as obtained from integration of the phase-averaged pressure distributions.

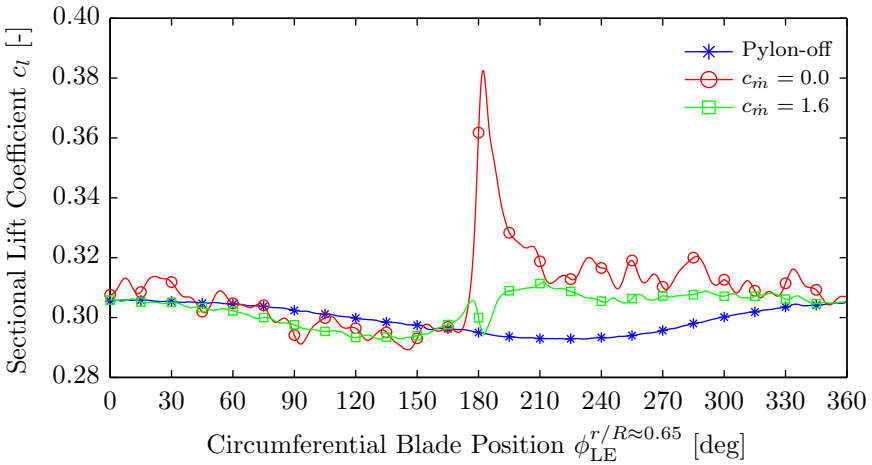

Figure 14. Effect of pylon installation on the sectional lift coefficient; $r/R \approx 0.65$, $J = 1.40$.

It can be seen in Fig. 14 that the installation of the pylon caused a surge in the blade lift during the wake encounter. Compared to the pylon-off case, the local loads were increased by approximately 30%. Application of blowing strongly reduced the pylon-installation impact, leading to a lift-coefficient history much closer to that measured for the isolated propeller. The data recorded for the pylon-off configuration again showed an oscillation with period equal to one rotation, confirming the angle-of-incidence effect discussed earlier.

The time histories plotted in Fig. 14 were used to compute the root-mean-square amplitude of the lift fluctuations. Figure 15 presents the resulting levels, as a function of the blowing coefficient. Apart from the intermediate thrust condition, also the low and high thrust settings are included. The data were normalized by the mean values of the lift coefficient at the respective operating points.

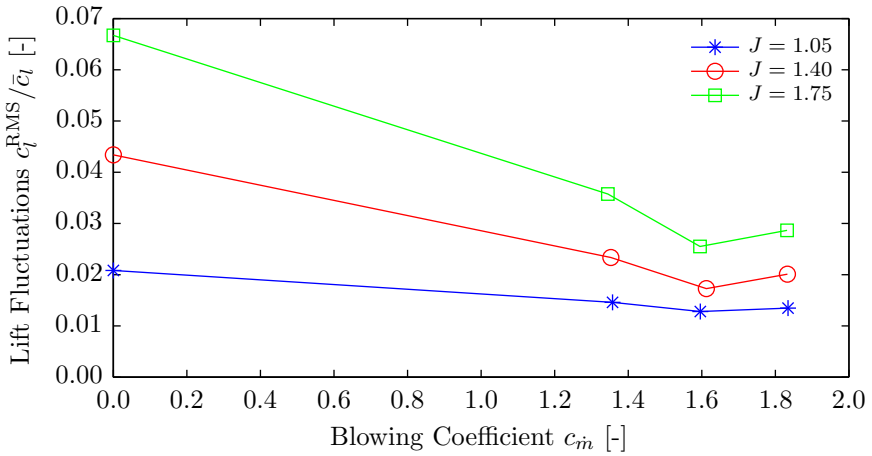

Figure 15. Lift fluctuations as a function of the blowing coefficient; $r/R \approx 0.65$.

Figure 15 displays a number of interesting aspects of the pylon–propeller interaction. For the unblown configuration, the installation impact increased with decreasing thrust setting. This was due to the increasing ratio of unsteady-to-steady blade loads and the growing relative importance of the velocity deficit in the pylon wake compared to the rotational velocity of the blades. The application of pylon trailing-edge blowing reduced the lift fluctuations at all propeller operating points. The smallest fluctuations were achieved at $c_{\dot{m}} = 1.6$, as expected considering the wake profiles shown in Fig. 9. At the lower blowing coefficient ($c_{\dot{m}} = 1.4$), the wake was not sufficiently filled yet, while at the highest blowing coefficient ($c_{\dot{m}} = 1.8$) the velocity overshoot on the wake centerline enhanced the overall lift oscillations.

In addition to the time-domain evaluations discussed above, the surface-pressure data were also analyzed in the frequency domain. For this purpose, the time histories were taken of the pressure sensor on the suction side of the blade at $x/c = 0.05$. Welch's method[17] was used to convert the raw signals into narrowband spectra with a frequency resolution of approximately 3 Hz. The results are presented in Fig. 16, in which the frequency is nondimensionalized with the rotational speed of the propeller. Markers are displayed at the tonal levels at integer multiples of the shaft frequency. Mains interference caused tonal components at multiples of 50 Hz. The resulting frequencies did not coincide with the considered multiples of the shaft frequency, while the amplitudes were only significantly present in the results recorded for the pylon-off configuration.

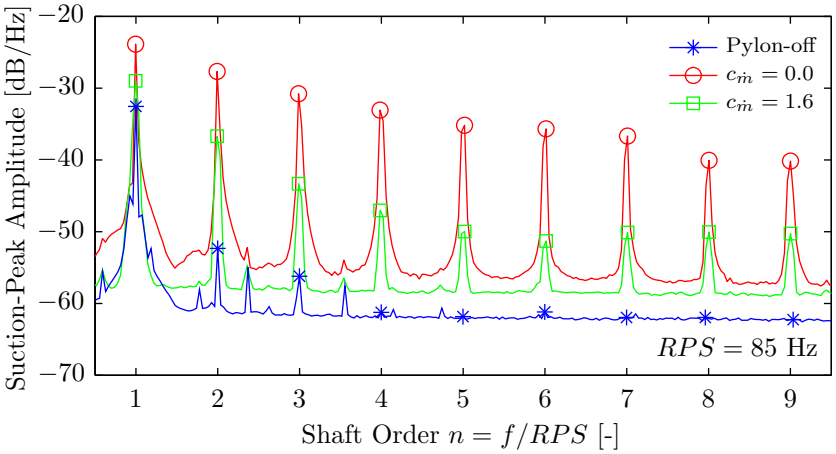

Figure 16. Frequency-domain representation of suction-peak pressure data; $x/c = 0.05$, $r/R \approx 0.65$, $J = 1.40$.

The spectra plotted in Fig. 16 underline the impulsive nature of the blade response for the unblown pylon-installed configuration. Clearly defined tonal components can be seen at all included multiples of the shaft order. For the pylon-off case, on the other hand, the spectrum was dominated by the fundamental tone at the shaft frequency due to the angle-of-incidence effect discussed before. Apart from the higher tonal amplitudes, Fig. 16 also reveals an increase of the broadband levels due to the installation of the pylon. This is attributed to the relatively high turbulence levels in the pylon-wake region when compared to the undisturbed flow, as seen in the sPIV data discussed in Ref. 7. Consequently, the random blade-load fluctuations were stronger for the case with the pylon present, explaining the increased broadband levels.

The application of blowing decreased the amplitudes of the tonal pressure fluctuations by reducing the severity of the wake encounter. Because of the remaining non-uniformities in the wake profile, however, the associated levels were not completely recovered towards those measured for the pylon-off configuration. Apart from the reduction of the harmonic components, also the broadband levels decreased by blowing. This was likely due to the reduction of the turbulence intensity in the blown pylon wake, as shown in Ref. 7.

Figures 11 through 16 demonstrate that the application of blowing reduces the unsteady blade loads caused by the installation of the pylon. To relate this to the beneficial effect of blowing on the pylon-wake characteristics, Fig. 17 plots the root-mean-square amplitudes of the lift variations as a function of the integral velocity deficit in the wake. Again the intermediate thrust condition is considered.

Figure 17 confirms the relation between the integral velocity deficit in the pylon wake and the unsteady blade loads caused by the wake encounter. The reduction of the deficit by blowing decreased the root-mean-square amplitude of the lift fluctuations by an average value of 55% when compared to the unblown configuration. This explains the efficacy of the pylon-blowing technique in reducing the noise penalty associated with the pylon-installation effects. The acoustic measurements performed in parallel during the same experiment, discussed previously in Ref. 7, confirmed this statement. Application of pylon blowing completely eliminated the noise penalty due to the installation of the pylon for the first three propeller tones.

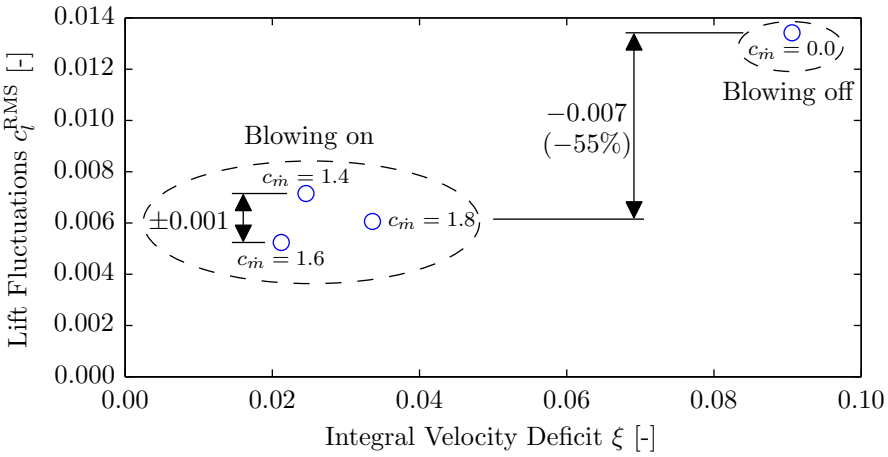

Figure 17. Lift fluctuations versus integral velocity deficit in the pylon wake; $r/R \approx 0.65$, $J = 1.40$.

C. Integral Blade Loads

The previous section established the impact of the pylon-wake encounter on the sectional blade-loading characteristics, and the efficacy of pylon trailing-edge blowing in reducing the pylon-installation effects. Now, attention is focused on the integral propeller performance, measured using the RSB. Table 2 compares the thrust coefficients recorded for the pylon-off and pylon-installed configurations. The data uncertainty was estimated by taking the standard deviation of the mean performance levels recorded during repeated measurements for the pylon-off configuration. Compared to the results presented previously in Ref. 7, the processing of the RSB data was modified to account for a linear shift in zero-loading offset during the measurements due to temperature effects. Also, the results are now based on averages over all available data points in the entire test program instead of single measurements.

Table 2. Effect of pylon installation on the time-averaged propeller thrust coefficient.

J	$C_T^{\text{Pylon-off}}$	$C_T^{\text{Pylon-on}}$
1.05	0.509 ± 0.001	0.510 ± 0.001
1.40	0.356 ± 0.003	0.357 ± 0.003
1.75	0.183 ± 0.008	0.187 ± 0.008

From the data provided in Table 2 it is concluded that the installation of the pylon hardly affected the time-averaged thrust coefficient. The installation impact was less than +2%, and fell within the measurement uncertainty at all advance ratios considered. Therefore, it was concluded that the effects of blowing on the mean propeller performance should be negligible as well, and thus are not further discussed in this paper.

To gain further insight into the effects of pylon installation on the propeller performance, spectral analysis was performed on the thrust-coefficient data. It was found that the RSB data contained spurious modes related to either shaft vibrations or resonance of the balance at most of the operating conditions considered, masking the phenomena related to the installation of the pylon. However, at the intermediate thrust setting ($J = 1.40$) the signal quality was sufficient to observe the installation effects. Figure 18 presents the phase-averaged thrust-coefficient data measured in this regime for the pylon-off and pylon-installed configurations, with and without blowing. The results were obtained by averaging the data recorded during 24 to 39 different runs (depending on the configuration), consisting of around 2,500 revolutions each. The measurement uncertainty was computed as the standard deviation of the mean values obtained from repeated measurements taken for the pylon-off configuration, and is indicated by the error bar in the top left of Fig. 18.

Figure 18 shows a clear six-peaks-per-revolution oscillation for the unblown pylon-installed configuration, corresponding to the periodic wake encounters. Despite the impulsive fluctuations of the sectional blade loads (Fig. 14), the development of the thrust coefficient was relatively smooth due to the phase-lag effects introduced by the large blade sweep. Also, it is possible that the response time of the RSB was insufficient to follow the sudden load change during the pylon-wake encounter, instead recording a more gradual response. The thrust-coefficient time histories for the pylon-off and blown pylon-installed configurations were

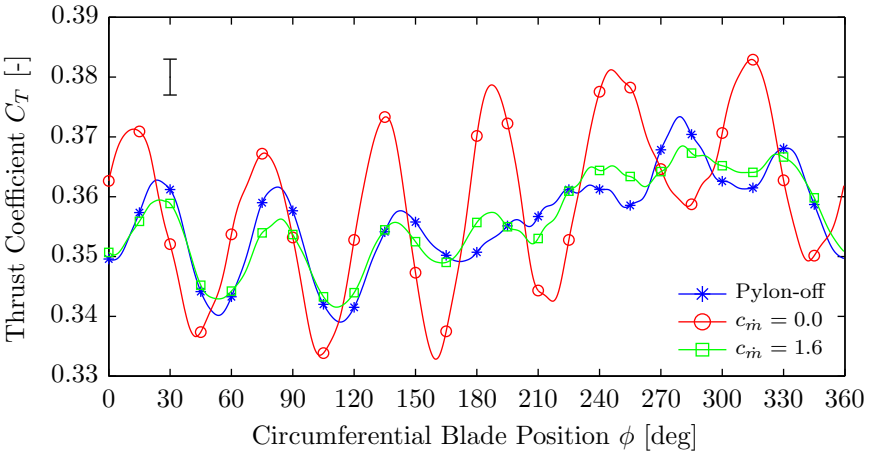

Figure 18. Effect of installation of the pylon on the phase-averaged thrust coefficient; $J = 1.40$.

comparable. For both cases, the root-mean-square amplitude of the thrust-coefficient variations was about half the value measured for the unblown pylon-installed configuration. This again confirms that application of the blowing system reduced the pylon-installation impact.

IV. Conclusions

A semi-installed pusher-propeller configuration was simulated by placing a tractor-propeller model downstream of a pylon. In such a configuration, the propeller inflow is perturbed by the pylon wake, introducing adverse installation effects. Pylon trailing-edge blowing was used to quantify the reductions of the interaction effects achievable by pylon-wake filling. Application of the blowing system decreased the velocity deficit in the wake region, thereby reducing the non-uniformity of the propeller inflow. At the optimal blowing rate, a decrease in integrated velocity deficit of 77% was achieved compared to the unblown case. A velocity overshoot occurred on the wake centerline due to the small thickness of the blowing slit in the pylon trailing edge and the limited mixing length between the pylon and the propeller.

The sudden drop in inflow velocity during the pylon-wake encounter results in an impulsive increase of the sectional angle of attack, causing a localized, rapid increase of the blade loads. The associated changes in the blade pressure distribution were concentrated near the leading edge of the blade. The unsteady nature of the perturbation problem introduced a slight phase lag in the blade response. The velocity-deficit reduction achieved by pylon blowing decreased the amplitude of the unsteady propeller blade loads, leading to a response comparable to that obtained for the isolated propeller. This explains the noise benefits of pylon trailing-edge blowing observed in parallel during the same experiment and also in previous studies. Despite the pronounced local impact on the sectional blade loads, the integral mean propeller performance was hardly affected by the installation of the pylon.

Acknowledgments

The results presented in this paper were obtained by the APIAN-INF research partners in the framework of the transnational access program organized by the ESWIRP consortium, as part of the ESWIRP project (European Strategic Wind tunnels Improved Research Potential). The research leading to these results has received funding from the European Union Seventh Framework Programme (FP7-INFRASTRUCTURE-2008-1) under grant agreement n° 227816.

The efforts of Hermann Holthusen during the preparation, execution, and processing of the test campaign are much appreciated. Christian Potma is thanked for designing the pylon-blowing system.

References

[1]Page, M. A., Ivey, D. M., and Welge, H. R., "Ultra High Bypass Engine Applications to Commercial and Military Aircraft," *SAE Technical Paper 861720*, 1986.

[2]Stürmer, A., Yin, J., and Akkermans, R., "Progress in aerodynamic and aeroacoustic integration of CROR propulsion systems," *The Aeronautical Journal*, Vol. 118, No. 1208, 2014, pp. 1137–1158.

[3]Farokhi, S., "Pressure-Time History of Pylon Wake on a Pusher Propeller in Flight," *Journal of Propulsion and Power*, Vol. 6, No. 6, 1990, pp. 758–768.

[4]Farokhi, S., Taghavi, R., and Wetzel, K. K., "Frequency-Domain Analysis of Fluctuating Pressure on a Pusher Propeller Blade Surface," *Journal of Aircraft*, Vol. 31, No. 1, 1994, pp. 42–48.

[5]Gentry, G. L., Jr., Booth, E. R., Jr., and Takallu, M. A., "Effect of Pylon Wake With and Without Pylon Blowing on Propeller Thrust," 1990, NASA-TM-4162, NASA Langley Research Center.

[6]Sinnige, T. and Veldhuis, L. L. M., "Pylon Trailing Edge Blowing Effects on the Performance and Noise Production of a Pusher Propeller," *52nd AIAA Aerospace Sciences Meeting*, 2014, National Harbor, MD, USA.

[7]Sinnige, T., Lynch, K. P., Ragni, D., Eitelberg, G., and Veldhuis, L. L. M., "Aerodynamic and Aeroacoustic Effects of Pylon Trailing Edge Blowing on Pusher Propeller Installation," *21st AIAA/CEAS Aeroacoustics Conference*, 2015, Dallas, TX, USA.

[8]Shivashankara, B. N., Johnson, D. P., and Cuthbertson, R. D., "Installation Effects on Counter Rotating Propeller Noise," *13th AIAA Aeroacoustics Conference*, 1990, Tallahassee, FL, USA.

[9]Ricouard, J., Julliard, E., Omaïs, M., Regnier, V., Parry, A. B., and Baralon, S., "Installation effects on contra-rotating open rotor noise," *16th AIAA/CEAS Aeroacoustics Conference*, 2010, Stockholm, Sweden.

[10]Paquet, C., Julliard, E., Genoulaz, N., Ricouard, J., and Spiegel, P., "Z08: low-speed aero-acoustic experimental characterization of open rotor installation on aircraft," *20th AIAA/CEAS Aeroacoustics Conference*, 2014, Atlanta, GA, USA.

[11]Fernando, R. and Leroux, M., "Open-Rotor low speed aero-acoustics: wind tunnel characterization of an advanced blade design in isolated and installed configurations," *20th AIAA/CEAS Aeroacoustics Conference*, 2014, Atlanta, GA, USA.

[12]Stürmer, A. and Yin, J., "Pylon Trailing Edge Blowing for the Control of CROR Unsteady Blade Loads," *New Results in Numerical and Experimental Fluid Mechanics VIII*, edited by A. Dillmann, G. Heller, H.-P. Kreplin, W. Nitsche, and I. Peltzer, Vol. 121 of *Notes on Numerical Fluid Mechanics and Multidisciplinary Design*, Springer Berlin Heidelberg, 2013, pp. 715–722.

[13]Polacsek, C., Spiegel, P., Boyle, F., Eaton, J., Brouwer, H., and Nijboer, R., "Noise Computation of High-Speed Propeller-Driven Aircraft," *6th AIAA/CEAS Aeroacoustics Conference and Exhibit*, 2000, Lahaina, HI, USA.

[14]Bousquet, J.-M. and Gardarein, P., "Recent improvements in Propeller Aerodynamic computations," *18th AIAA Applied Aerodynamics Conference*, 2000, Denver, CO, USA.

[15]Philipsen, I., Hoeijmakers, H., and Hegen, S., "An Overview of Advanced Propeller Simulation Tests in the German Dutch Wind Tunnels (DNW)," *22nd AIAA Aerodynamic Measurement Technology and Ground Testing Conference*, 2002, St. Louis, MO, USA.

[16]Crozier, P., "APIAN Installed Tests in the ONERA S1MA Wind Tunnel," *39th AIAA Aerospace Sciences Meeting & Exhibit*, 2001, Reno, NV, USA.

[17]Welch, P. D., "The Use of Fast Fourier Transform for the Estimation of Power Spectra: A Method Based on Time Averaging Over Short, Modified Periodograms," *IEEE Transactions on Audio and Electroacoustics*, Vol. 15, No. 2, 1967, pp. 70–73.